

α -particle condensation: A nuclear quantum phase transitionJ.-P. Ebran^{1,2,*}, M. Girod^{1,†}, E. Khan^{3,‡}, R. D. Lasserri^{4,§} and P. Schuck^{3,||}¹CEA, DAM, DIF, F-91297 Arpajon, France²Université Paris-Saclay, CEA, Laboratoire Matière en Conditions Extrêmes, 91680 Bruyères-le-Châtel, France³Institut de Physique Nucléaire, Université Paris-Sud, IN2P3-CNRS, Université Paris-Saclay, F-91406 Orsay Cedex, France⁴ESNT, CEA, IRFU, Département de Physique Nucléaire, Université Paris-Saclay, F-91191 Gif-sur-Yvette, France

(Received 16 December 2019; revised 17 May 2020; accepted 8 May 2020; published 6 July 2020)

When the density of a nuclear system is decreased, homogeneous states undergo the so-called Mott transition towards clusterized states, e.g., α clustering, both in nuclei and in nuclear matter. Here we investigate such a quantum phase transition (QPT) by using microscopic energy density functional calculations with the relativistic and the Gogny approaches on the diluted ^{16}O nucleus. The evolution of the corresponding single-particle spectrum under dilution is studied, and a Mott-like transition is predicted at about 1/3 of the saturation density. A complementary study of quartet condensation and the corresponding macroscopic QPT is undertaken in infinite matter.

DOI: [10.1103/PhysRevC.102.014305](https://doi.org/10.1103/PhysRevC.102.014305)**I. INTRODUCTION**

Fermi systems are the host of various phenomena yet to be fully explored. One of the most recent exciting features which has been revealed is the exotic arrangements stabilized by the existence of internal degrees of freedom in N -component Fermi systems with $N > 2$ [1–4]. Molecular configurations made of bound states of N fermions enrich the celebrated crossover [5] between a Bardeen-Cooper-Schrieffer (BCS) superfluid phase to the Bose-Einstein condensation (BEC) of bosonic bound states of two fermions that characterizes two-component Fermi gases with an attractive s -wave interaction. Nucleons being assigned to spin and isospin SU(2) doublet, atomic nuclei fall in the category of four-component self-bound Fermi systems. Attractive s -wave interactions in the singlet-even ($S = 0, T = 1$) and the triplet-even ($S = 1, T = 0$) channels— S and T stand respectively for the total spin and isospin momenta of the two-nucleon system—with almost similar strengths give rise to various types of superfluid behavior. Indeed, even though the nucleon-nucleon interaction strength is fixed, the effective strength of the pairing interaction scales as the inverse s -wave scattering length a_s , normalized by the Fermi momentum k_F [$\approx (k_F a_s)^{-1}$], such that the coupling regime can be tuned by varying the nucleon density $\rho \propto k_F^3$. In the weak coupling regime (near and beyond the saturation density $\rho_0 \approx 0.16 \text{ fm}^{-3}$), the dominant superfluid instability takes the form of a BCS quasi-long-

range order and involves proton-proton, neutron-neutron, or proton-neutron (depending on the matching of neutron and proton Fermi levels) Cooper pairs [6,7]. Moving towards the strong coupling regime (at subsaturation density), calculations in infinite symmetric nuclear matter [8] suggest that the dominant superfluid order is not a BEC phase of bosonic dimers (deuterons), but rather a condensation phase of quartets—four-fermion molecular objects with zero total spin and isospin. For decreasing densities, infinite nuclear matter hence undergoes a phase transition to α -particle condensation [8–10]. That is, nuclear matter lowers its energy by taking advantage of the nuclear cohesion, i.e., by forming localized clusters that recover saturation density, rather than remaining in a dilute homogeneous phase. Because this happens at zero temperature, it can be dubbed a quantum phase transition (QPT), with the density being the control parameter.

How such features translate in finite nuclei triggered several research works (see, e.g., Refs. [11–16]). Unlike homogeneous systems, finite nuclei naturally display large fluctuations of their mass density around the equilibrium value ρ_0 , in both their ground state and their excited states. There, a combination of energetics consideration and Pauli principle is expected to trigger a QPT from a dilute homogeneous configuration to a clusterized configuration, endowing the spectroscopy of relatively light nuclei with clusterized structures [17–20]. For instance, the famous Hoyle state, important for ^{12}C production in the universe, could be interpreted as a three- α gas state where the α 's occupy with their center-of-mass (c.m.) motion up to 70–80% of the lowest 0S wave function while all other states have an occupation probability more than a factor of 10 down (see, e.g., Ref. [21]). In that sense, the Hoyle state can be qualified as a finite-size α -particle condensate. However EDF and geometrical approaches end up with α clusters in a much more robust configuration [22–24] (see

*jean-paul.ebran@cea.fr

†michel-g.girod@cea.fr

‡khan@ipno.in2p3.fr

§raphael.lasserri@cea.fr

||schuck@ipno.in2p3.fr

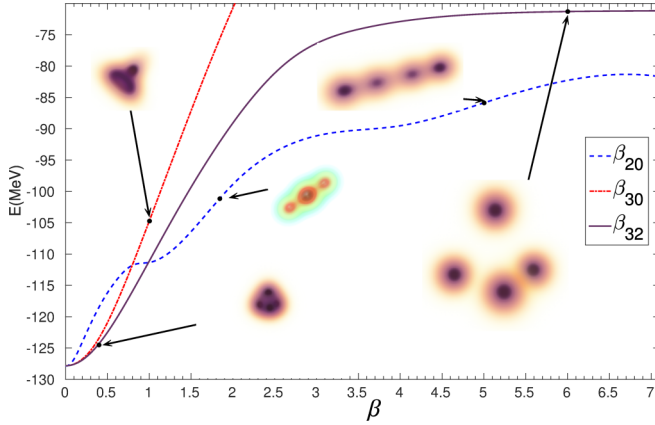


FIG. 1. Binding energy of ^{16}O as a function of a deformation parameter (axial quadrupole, axial octupole, and tetrahedral ones), calculated within the CEDF at the SR level with the DD-ME2 parametrization [44]. The inserts display the three-dimensional nucleonic density in the intrinsic frame of the nucleus for various values of the deformation parameter.

also Ref. [25] for a recent experimental investigation of this issue and Ref. [26] for a discussion of α -cluster structures as a manifestation of supersolidity). It should be noted that the action of the Pauli principle is quite similar in both cases (gas or molecular states) so converging results will be reached from both approaches. Beyond these interpretations, the size of the Hoyle state is extended to 3–4 times the volume of the ^{12}C ground state [27,28], showing that Hoyle and ground states live in two completely different phases, one dilute, the other dense.

In this work, we want to further substantiate the QPT scenario of α clustering for the case of ^{16}O through complementary perspectives. A microscopic analysis based on the EDF approach is given in Sec. II, where both covariant and Gogny functionals are used. Constrained Hartree-Fock-Bogoliubov (HFB) calculations for ^{16}O are performed, the constraint being on the radius of ^{16}O while the system is imposed to stay globally spherical. That is, ^{16}O can break up into clusters while the system still stays spherical on average. Section III provides an analysis of the occurrence of α condensation in nuclear matter through the explicit treatment of four-nucleon correlations.

II. EDF APPROACH TO QUANTUM PHASE TRANSITION IN FINITE NUCLEI

A. Clustering in the language of nuclear EDFs

The description of cluster configurations in finite nuclei based on nuclear EDFs or the mean-field approach has a long history [14,15,19,20,22,29–43]. To account for the properties of α -correlated states, these approaches do not introduce explicit four-body correlations. Rather, they involve an order parameter associated with α clustering, i.e., a collective field whose fluctuations cause nucleons to gather into α subunits. The multipolar mass moments $Q_{\lambda,\mu}$ provide an example of such order parameters (see Fig. 1). Indeed, a nonzero value for $Q_{\lambda,\mu}$ is a necessary (yet not sufficient) condition for the

emergence of localized substructures in nuclei, while the extreme scenario of all nucleons aggregating into α degrees of freedom can be described in terms of a spontaneous breaking of the rotational symmetry $O(3)$ displayed by the nuclear Hamiltonian down to a discrete point group that dictates the geometrical configuration of the α particles.

The link between deformation and cluster formation is well understood and has already been investigated in the simple case where the nuclear confining potential is approximated by a harmonic oscillator (HO) one [45–49]. In essence, the degeneracies of the energy levels of an N -dimensional isotropic (spherical configuration) HO are in one-to-one correspondence with the irreducible totally symmetric representations of $SU(N)$. Similarly, the quantum states of an N -dimensional anisotropic oscillator (deformed configuration) with commensurate frequencies (i.e., rationally related frequencies ω_i such that $k_i\omega_i = \omega$ and k_i are relatively prime integers) enjoy degeneracy spaces that also correspond to the representations of $SU(N)$, with the important difference that unlike the isotropic oscillator, a given representation occurs not singly but with a multiplicity $\prod_i k_i$. As a consequence, the symmetries of the corresponding many-particle wave function can be described by independent copies of $SU(3)$ irreducible representations (irreps), suggesting that the shell structure of the anisotropic HO with commensurate frequencies is that of smaller overlapping spherical HOs. In other words, the corresponding many-body system has a susceptibility to distribute its total mass among multiple spherical fragments, that is to say, to clusterize.

This simple picture survives in a more realistic description where the confining nuclear potential is determined self-consistently, as illustrated in Fig. 1: ^{16}O total binding energy, computed at the single-reference (SR) level of the covariant energy density functional (CEDF) approach (also referred to as the mean-field level), is displayed against different constrained deformation parameters, namely, the axial quadrupole $(\lambda, \mu) = (2, 0)$, the axial octupole $(\lambda, \mu) = (3, 0)$, and the triaxial octupole $(\lambda, \mu) = (3, 2)$ modes. ^{16}O intrinsic densities are also displayed for values of interest of the deformation parameters. The global minimal energy is found at the spherical point, owing to the p -shell closure in ^{16}O . Small values of the deformation parameters (<1) correspond to deformed shapes where nucleons are roughly homogeneously distributed: prolate cigarlike shape along β_{20} , pearlike configuration along β_{30} , and tetrahedral distribution along β_{32} . The energy is rather stiff in the β_{20} direction, contrary to the octupole directions, especially the triaxial one: for $\beta_{32} \approx 0.3$ where the tetrahedral shape is already well developed, the energy loss with respect to the spherical configuration is only 3 MeV. Projection on both angular momentum and parity as well as mixing within the generator coordinate method (GCM) may therefore induce tetrahedral correlations in the ground state of ^{16}O and yield several rotation-vibration excited states that can be classified according to the irreps of the discrete tetrahedral group T_d , along the lines of Ref. [24]. For large deformation parameters, Fig. 1 involves binary cluster structures, e.g., $\alpha + ^{12}\text{C}$ at $\beta_{30} \approx 1$, followed by ternary cluster structures ($^8\text{Be} + 2\alpha$ at $\beta_{20} \approx 1.7$). For extreme values of the deformation parameters where the nuclear radius is

large, hence the average density is low enough for Pauli blocking effects to be suppressed, ^{16}O displays a fully clustered structure with four α 's in linear ($\beta_{20} \approx 5$) or tetrahedral ($\beta_{32} \approx 6$) configurations.

B. Density-induced quantum phase transition

In this subsection, we want to establish the transformation from a delocalized configuration to a clustered one as a QPT. For that purpose, we do not explore the manifold of constrained mean-field solutions parametrized by some multipolar mass moments $Q_{\lambda\mu}$ acting as collective coordinates, like the one-dimensional potential energy surface displayed in Fig. 1. Such an approach, complemented by a post-mean-field treatment, e.g., the GCM, would yield the spectroscopy of the system with states possibly displaying delocalized or clustered structures or a coexistence of both [19,20]. Rather, we want to start from a homogeneous configuration where all the multipolar mass moments are zero ($Q_{\lambda\mu} = 0 \forall \lambda, \mu$) and continuously diluting the system by, e.g., constraining its rms radius while imposing a zero global quadrupole mass moment Q_{20} [14,15] (see Fig. 2). The transition between two distinct quantum phases, namely, a homogeneous configuration and a clustered one, visible in the density profile of the system, is accompanied by the onset of some $Q_{\lambda\mu}$ with $\lambda > 2$ (we remind the reader that the quadrupole moment is constrained to zero). Such a transition is expected beyond a critical rms radius, or equivalently below a critical mean density called the Mott density.

We investigate the transition from the homogeneous to the clustered configurations by describing the isotropic inflation of ^{16}O within both the CEDF and Gogny EDF approaches. The corresponding constrained mean-field equations are solved in a HO basis with 11 major shells. A careful analysis of the convergence and nonartificial nature of the solution with respect to the HO basis parameters must be undertaken, especially when addressing exotic dilute (with a large constrained rms radius) configurations. Indeed, some values of the parameter $\hbar\omega$ may lead to unphysical lower-energy configurations where some of the nucleons remain tightly packed at the center of the nucleus while the remaining nucleons are sparsely distributed around this dense core. We retain values of $\hbar\omega$ that minimize the energy of the system and at the same time lead to a regular decrease of the density. These features are illustrated in Fig. 2. Figure 2(a) displays the radial density of ^{16}O for several constrained radii in the relativistic case. The parameter of the HO basis yielding the lowest energy constrained configurations and at the same time allowing a regular decrease of the density is found to be $\hbar\omega = 13$ MeV. Figure 2(b) shows the density profile obtained in the nonrelativistic case, where the colors distinguish between several values of $\hbar\omega$. For $\hbar\omega < 19$ MeV, the constraint on the radius, taken between 2.4 and 3.8 fm, does not lead to a regular decrease of the density at the center of the nucleus. As a matter of fact, the nucleus increases its radius by expanding a low-density nucleon cloud surrounding a quasi-constant-density nucleon core (red dashed and green dotted curves). These features are not appropriate. A regular decrease of the central density is only obtained for $\hbar\omega \approx 19$ MeV (blue solid

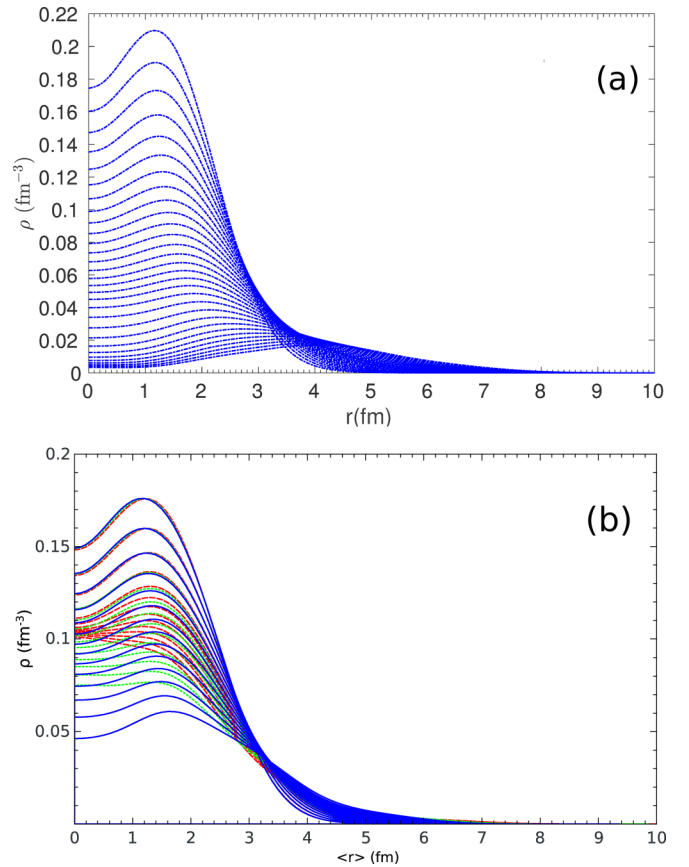


FIG. 2. ^{16}O nucleon radial density for rms radii constrained (a) from 2.4 to 5.3 fm within symmetry-restricted RMF calculations with the DD-ME2 parametrization and (b) from 2.5 to 3.8 fm within HFB calculations with the Gogny D1S parametrization [50]. Relativistic calculations (a) are performed in a HO basis with 11 shells and $\hbar\omega = 13$ MeV. Nonrelativistic calculations (b) are also performed in a HO basis with 11 shells but with $\hbar\omega = 15$ MeV (red dashed line), 17 MeV (green dotted line), and 19 MeV (blue solid line).

curves) within Gogny D1S calculations, which we adopt hereafter in the nonrelativistic case as far as spherical shapes are concerned. In the case of clustered configurations, the value of optimal $\hbar\omega$ with respect to the HFB binding energy is 11 and 8 MeV for the relativistic and nonrelativistic calculations, respectively. Note that there is no specific reason for the $\hbar\omega$ parameter to be the same in the covariant and nonrelativistic calculations.

Setting the HO basis parameters to their relevant values, the ^{16}O binding energy is computed as a function of the constrained rms radius within both the CEDF and the Gogny EDF approaches and is displayed in Fig. 3. Both types of calculations remarkably agree on the transition between a dilute spherical configuration (red curves with circle markers) and a four- α phase where the α clusters are distributed at the vertices of a tetrahedron past a critical rms radius. To analyze in more detail how ^{16}O rearranges itself during the QPT, several types of calculations are performed in the covariant case [Fig. 3(a)]. The conclusions drawn here can be trans-

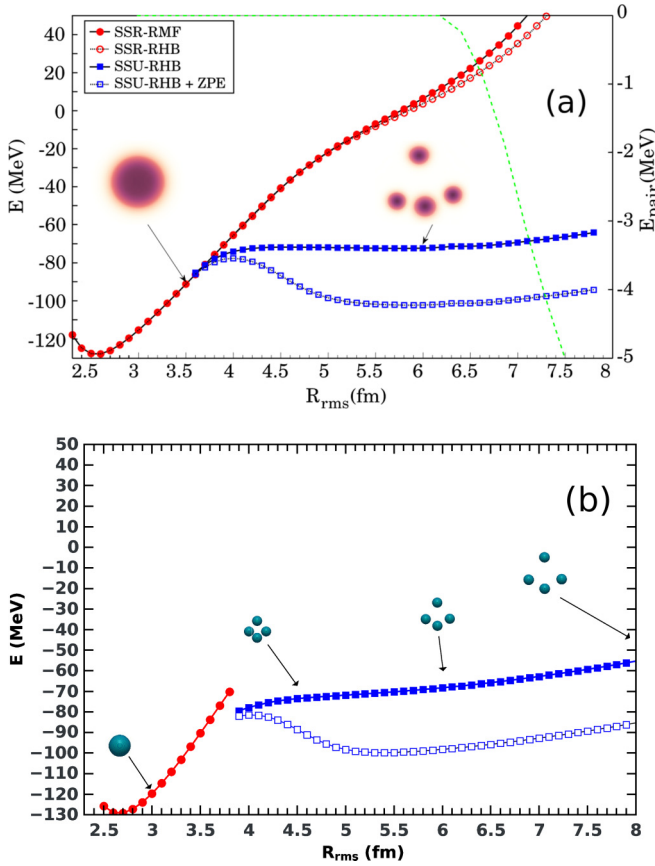


FIG. 3. Self-consistent binding energy of ^{16}O computed at the SR level of (a) the CEDF with the DD-ME2 parametrization and (b) the EDF with the Gogny D1S parametrization vs the constrained rms radius. In panel (a) curves with red circle symbols correspond to spherical configurations obtained in a HO basis with 11 shells and $\hbar\omega = 13$ MeV, while the blue square symbol curves correspond to a tetrahedral arrangement obtained in a HO basis with 11 shells and $\hbar\omega = 11$ MeV. The green dashed line displays the pairing energy associated with superfluid spherical configurations (red open circle symbols). Likewise, in panel (b) red (circle symbols) and blue (square symbols) correspond to spherical and tetrahedral configurations, respectively, and were obtained in a HO basis with 11 shells and $\hbar\omega = 19$ and 8 MeV, respectively. In both cases, the blue open square symbol curve corrects the mean-field energy with the zero-point energy contribution, and the inserts display ^{16}O intrinsic density at the corresponding constrained radii. See text for detailed explanations.

posed to the nonrelativistic case. For the sake of conciseness, we hence restrict the detailed analysis to the CEDF approach. In Fig. 3(a), the curve with red solid circle markers corresponds to a SR-CEDF calculation where we enforce spherical symmetry [i.e., no spatial spontaneous symmetry breaking (SSB) can occur] as well as the global $U(1)$ invariance (i.e., no pairing correlations can develop). We refer to this case as spatial-symmetry-restricted relativistic mean field (SSR-RMF). Relaxing the enforcement of $U(1)$ symmetry, i.e., still restricting the spatial symmetry to the spherical one, but letting the system free to break the $U(1)$ invariance signaling the development of pairing correlations, yields the curve

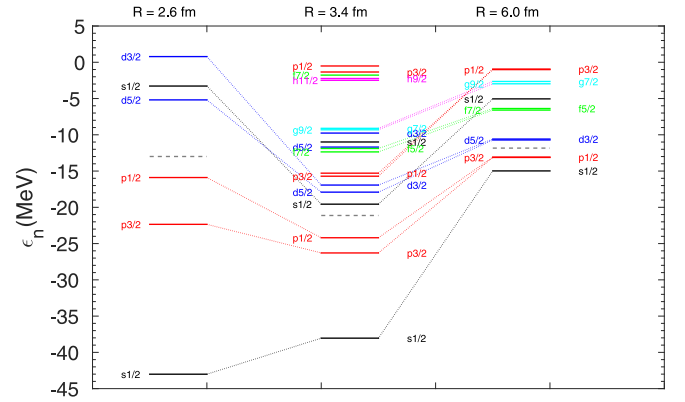


FIG. 4. ^{16}O neutron single-particle levels associated with SSR-RMF calculations with the DD-ME2 parametrization constrained at $R = 2.6, 3.4,$ and 6.0 fm.

with red open circle markers: this is the spatial-symmetry-restricted relativistic Hartree Bogoliubov (SSR-RHB) case. For this type of calculation, the green dashed line displays the corresponding pairing energy of the system. Finally, relaxing all the symmetry restrictions, both spatial and internal (with, however, the constraint $\beta_{20} = 0$ ensuring an isotropic inflation of the nucleus), yields the curves with blue square markers (solid and open markers). This case is referred to as spatial-symmetry-unrestricted relativistic Hartree Bogoliubov (SSU-RHB). In the curve with the square open symbols, the zero-point energy, computed as in Ref. [14], is subtracted from the SSU-RHB energy.

Let us first analyze the SSR-RMF case, by looking at the neutron single-particle (sp) orbitals for three different constrained radii (see Fig. 4): $R = 2.6$ fm (equilibrium configuration), $R = 3.4$ fm [just before the separation of the different curves in Fig. 3(a)], and $R = 6.0$ fm. Diluting ^{16}O causes a drastic reduction of the valence neutron gap from 10.71 MeV at $R = 2.60$ fm to 4.63 MeV at $R = 3.40$ fm and 2.36 MeV at $R = 6.0$ fm. The sp spectrum gets shrunk and all spin-orbit partners eventually become degenerate. These features can be understood by looking at the radial dependence of two combinations of the scalar and timelike nucleon self-energies S and V (Fig. 5). The combination $V + S$ defines the mean potential where independent nucleons evolve in the mean-field picture. From a typical depth of -75 MeV at the equilibrium configuration, the confining potential becomes shallower as the constrained radius increases until reaching -10 MeV at $R = 6.0$ fm. Likewise, the other combination $V - S$, whose derivative (with a prefactor of $1/M^2$ and M being the nucleon mass) governs the spin-orbit splitting, gets weaker as the radius increases, restoring the spin $SU(2)$ symmetry of the Dirac Hamiltonian and therefore causing spin-orbit partners to be degenerate.

Such a reduction of the Fermi gap opens room for the development of nondynamical correlations. Indeed, ^{16}O becomes a near-degenerate system; i.e., excited particle-hole (p-h) configurations have energies close to the fundamental one, such that the system will rearrange itself in a nonperturbative way to lift the (near) degeneracies.

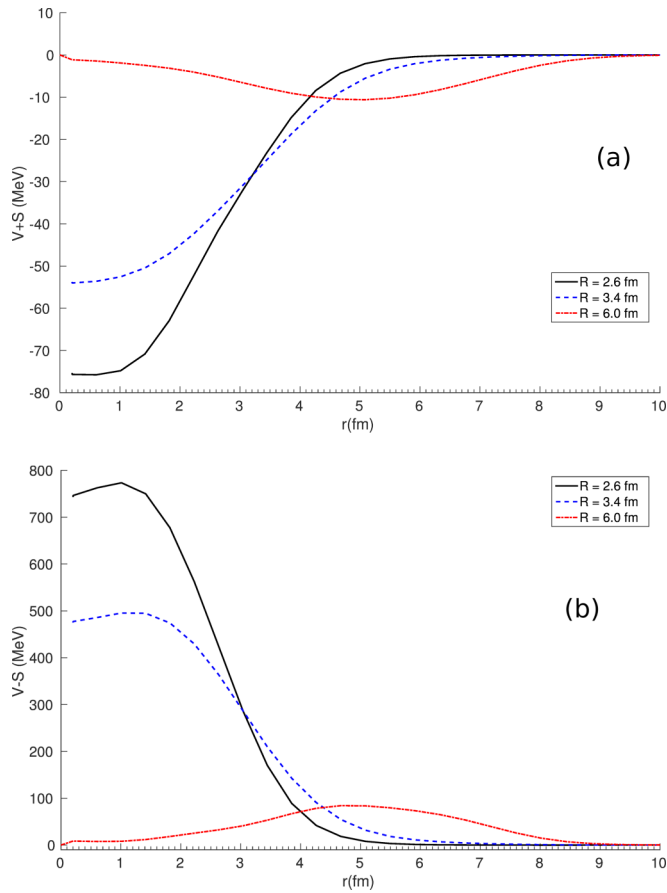


FIG. 5. Radial evolution of combinations [(a) $V + S$, (b) $V - S$] of the scalar (S) and timelike (V) nucleon self-energies in ^{16}O for radii constrained at $R = 2.6, 3.4,$ and 6.0 fm.

A possible strategy consists in developing pairing correlations. At the SR level, the onset of pairing correlations is signaled by the spontaneous breaking of the global $U(1)$ group associated with the conservation of the nucleon number. From the corresponding SSR-RHB calculations displayed Fig. 3(a), the normal to superfluid QPT occurs at $R = 3.8$ fm, even if a sensible effect on the binding energy has to wait for radii greater than $R = 5.5$ fm. Such a QPT translates into the opening of a gap in the quasiparticle (qp) spectrum of ^{16}O . At $R = 6.0$ fm, the gap in the neutron qp spectrum jumps from 2.2 MeV in the SSR-RMF case to 4.1 MeV in the SSR-RHB one, with a pairing energy ≈ -8 MeV. As one can see from the small impact on ^{16}O binding energy [Fig. 3(a)], lifting p-h near degeneracies by developing pairing correlations seems rather ineffective. This is due to the large-energy splitting between the d and f orbitals that hinders the scattering of Cooper pairs, as shown by the occupation numbers of the canonical neutron sp levels in Fig. 6 (SSR-RHB case).

A more effective strategy to lift the degeneracies is to develop angular correlations. From the SSU-RHB calculations, a Mott-like QPT is observed at a critical radius of $R_c = 3.7$ fm, that is, a mean density of $\rho_{\text{Mott}}/\rho_0 = (R_{\text{eq}}/R_c)^3 \approx 0.35$, or $\rho_{\text{Mott}} \approx \rho_0/3$. At such a low density, the Pauli principle does

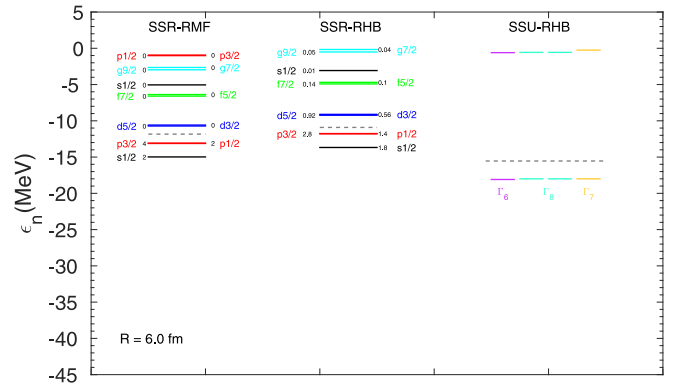


FIG. 6. ^{16}O neutron canonical single-particle levels computed at $R = 6.0$ fm with the DD-ME2 parametrization in the SSR-RMF, SSR-RHB, and SSU-RHB cases.

not prevent anymore the formation of α bound states, which is energetically preferred, because it takes advantage of the strong nuclear cohesion (the clusters recover a density closed to the saturation one). The transition hence occurs between a phase where nucleons are delocalized in a dilute spherical volume (the maximal value of the nucleon density is 0.046 fm^{-3} at $R = 3.40$ fm), for which the multipolar moments are zero, and a phase where nucleons are localized in four- α -like degrees of freedom at saturation density and arranged according to a tetrahedral configuration (the first nonzero multipole moment is Q_{32}). For such a tetrahedral configuration, no pairing correlations develop; i.e., the global $U(1)$ symmetry remains unbroken.

As mentioned above, the nonrelativistic Gogny EDF calculations [Fig. 3(b)] show remarkable similarities with the relativistic case [Fig. 3(a)]. The same transition between a spherical homogeneous configuration and localized tetrahedral configurations occurs, however, slightly later at $R_c = 3.9$ fm, or equivalently a mean density of $\rho_{\text{Mott}}/\rho_0 = (R_{\text{eq}}/R_c)^3 \approx 0.33$, i.e., again $\rho_{\text{Mott}} \approx \rho_0/3$. In the nonrelativistic calculations, a break is observed between the curve related to the spherical configurations (in red circles) and those for the tetrahedral configurations (in blue squares). The discontinuity occurs at the radius beyond which the spherical density evolves into a four- α -like configuration and stems from different values for the optimal $\hbar\omega$ in the spherical configuration case ($\hbar\omega = 19$ MeV) and in the tetrahedral one ($\hbar\omega = 12$ MeV). For the latter, the nucleus increases its radius by placing the α 's further apart, as illustrated in the inserts.

The many-faceted nature of the ^{16}O spectrum, and the presence of tetrahedral configurations in particular, has long been discussed [24,51–58]. We insist however on the fact that we do not seek a description of ^{16}O spectroscopy, but rather to characterize the density-induced QPT from a homogeneous to a clusterized configuration, that is, in the case of ^{16}O , from a spherical distribution of delocalized nucleons to a clusterized state of four α 's arranged according to a tetrahedron. The corresponding SSB of the rotational group $O(3)$ down to the (double) point group T_d yields a bandlike structure for the ^{16}O sp spectrum (see the SSU-RHB case of Fig. 6): the neutron

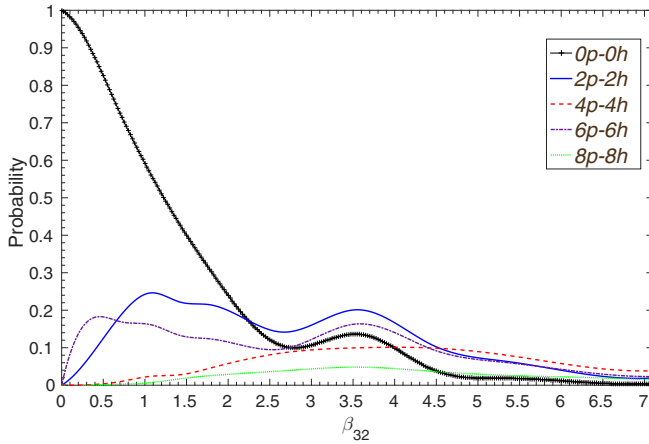


FIG. 7. Probability to find n -particle- n -hole states belonging to the $O(3)$ irreps in the tetrahedral SD state as a function of the nonaxial octupole deformation parameter β_{32} .

and proton sp orbitals assemble into two bunches of four near-degenerate orbitals separated by a huge gap of 17.4 MeV.

C. Analysis of nonaxial octupolar correlations

These features can be understood based on the properties of the group T_d [51,59–62]. In a tetrahedrally symmetric confining potential, the nucleon orbitals can be classified along the irreps of the group T_d (the so-called Γ_6 , Γ_7 , and Γ_8 irreps [59]). The correlations grasped by going through a tetrahedral deformation can be translated in the language of p-h excitations on top of a symmetry-preserving reference state by computing the overlaps $\langle \Phi_i^{\text{sph}} | \Phi_0^{\text{tetra}}(\beta_{32}) \rangle$ between the tetrahedrally deformed Slater determinant (SD) $|\Phi_0^{\text{tetra}}(\beta_{32})\rangle$ (the tetrahedral closed-shell configuration involving the Γ_6 , Γ_7 , and Γ_8 states) and spherical SDs $|\Phi_i^{\text{sph}}\rangle$ [both ground-state ($i = 0$) and p-h excitations ($i > 0$) in a valence space spanning the $1s1/2$ to the $1f5/2$ states] for various values of the order parameter β_{32} (Fig. 7).

The contribution of the spherical closed-shell configuration (0p-0h state) drops rapidly as the tetrahedral deformation increases. Collective excitations, in particular 2p-2h and 6p-6h ones, quickly become dominant, meaning that the amplitude excitations from the p shell to sd shells do not describe the total correlated wave function in a satisfactory manner, but one eventually needs to account for pf shell states as well as holes in the s state. It should be noted that the probabilities displayed in Fig. 7 do not add up to 1 because of the too small valence space.

The role played by the orbitals beyond the p and sd shells can be further understood by comparing the shape of the spherical canonical orbitals with the tetrahedral ones (Fig. 8). The four near-degenerate tetrahedral orbitals Γ_6 , Γ_7 , and Γ_8 (doubly degenerate) share the same partial density that resembles four α 's arranged in a tetrahedral configuration. To illustrate how spherically symmetric nucleonic shells combine in such tetrahedrally deformed orbitals, let us focus on the Γ_6 level. From the decompositions of the irreps of the full rotation group into irreps of the group T_d

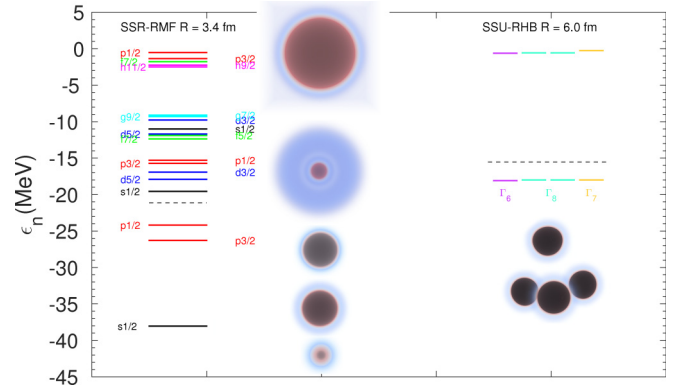


FIG. 8. ^{16}O neutron single-particle levels in the SSR-RMF case with $R = 3.4$ fm and in the SSU-RHB case with $R = 6.0$ fm computed with the DD-ME2 parametrization. The inserts display the partial densities associated with the $1s1/2$, $1p3/2$, $1p1/2$, $2s1/2$, and $1f7/2$ orbitals from bottom to top in the SSR-RMF case and for the Γ_6 , Γ_7 , and Γ_8 orbitals that share the same shape.

[59], the irreps compatible with Γ_6 are $D_{\frac{1}{2}}^+$, $D_{\frac{7}{2}}^+$, etc., for the positive parity case and $D_{\frac{3}{2}}^-$, $D_{\frac{7}{2}}^-$, etc., for the negative parity one. The corresponding lowest energy levels at $R = 3.4$ fm can be read from Fig. 8: the occupied $1s1/2$ orbital and unoccupied $2s1/2$, $1f7/2$, and $1f5/2$ orbitals (the p and d shells are not compatible with Γ_6). Superpositions of these (at least) four spherically symmetric orbitals are needed to yield a tetrahedrally shaped Γ_6 orbital. The latter having a zero contribution at the center of the nucleus, one first needs a mixture between the $1s1/2$ and $2s1/2$ orbitals, which belong to the Γ_6 subspace, to cancel the density at the origin. The resulting density is still isotropically distributed in space. To localize the nucleons occupying the Γ_6 orbital into α 's in a tetrahedral configuration, superposition with f states is also needed (because the p and d shells only involve the Γ_7 and Γ_8 irreps). Figure 9 illustrates this statement by splitting the

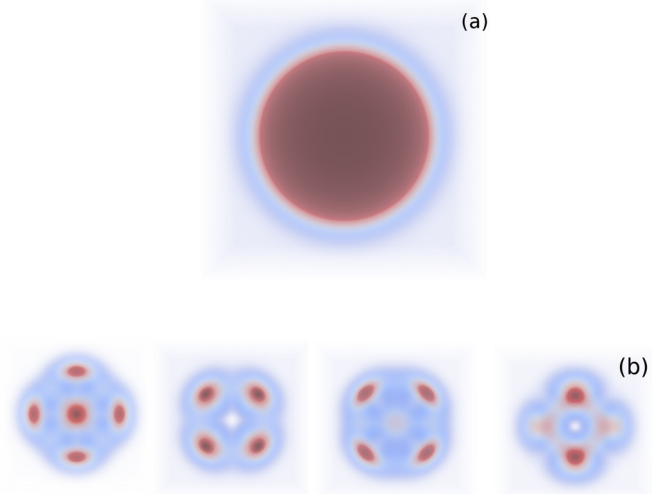


FIG. 9. $1f7/2$ partial density (a) and its decomposition on $m = 1/2, 3/2, 5/2$, and $7/2$ (b).

$1f7/2$ partial density into its magnetic $m = 1/2, 3/2, 5/2$, and $7/2$ degenerate components.

Finally, the structure of the tetrahedrally deformed sp spectrum (the SSU-RHB case of Fig. 6) can be interpreted by employing the language of quantum chemistry. The four tetrahedrally symmetric orbitals (Γ_6, Γ_7 , and the doubly degenerate Γ_8) can be expressed as a linear combination of localized Gaussian-type ‘‘atomic’’ orbitals ϕ_i ($i = 1, 2, 3, 4$) [63]; here $1s$ orbitals are associated with the α -particle ground state. The coefficient of the linear combination can be determined, e.g., within the Hückel approximation, yielding

$$\begin{aligned}\Gamma_6 &= \frac{1}{2}(\phi_1 + \phi_2 + \phi_3 + \phi_4), \\ \Gamma_7 &= \frac{1}{2}(\phi_1 - \phi_2 - \phi_3 + \phi_4), \\ \Gamma_8(1) &= \frac{1}{2}(\phi_1 + \phi_2 - \phi_3 - \phi_4), \\ \Gamma_8(2) &= \frac{1}{2}(-\phi_1 + \phi_2 - \phi_3 + \phi_4),\end{aligned}\tag{1}$$

with the eigenenergies

$$\begin{aligned}E_6 &= \epsilon - 3\mu, \\ E_7 &= \epsilon + \mu, \\ E_8(1) &= E_7, \\ E_8(2) &= E_8(1) = E_7,\end{aligned}\tag{2}$$

where ϵ and $-\mu$ respectively denote the energy kernels \mathcal{H}_{ii} and \mathcal{H}_{ij} (where the i th and j th atomic sites are adjacent) between the atomic orbitals located on the vertices of a tetrahedron. At $R = 6.0$ fm the energies of the Γ_i ($i = 6, 7$, and 8), $E_6 = -18.090$ MeV and $E_7 = E_8(1) = E_8(2) = -18.004$ MeV (see Fig. 8), lead to identifying the energy of the $1s$ α state, $\epsilon = -18.004$ MeV, as well as the nondiagonal energy kernel $\mu = 0.086$ MeV. Taking into account the ≈ 10 MeV correction coming from the zero-point energy contribution (blue open square curve in Fig. 3), the energy of the $1s$ α state drops to ≈ -28 MeV, in agreement with the binding energy of ${}^4\text{He}$. On the other hand the energy gap of 17.4 MeV between occupied and unoccupied states of the tetrahedrally deformed sp spectrum is of the order of the lowest excitation energy of the α particle (20.2 MeV), suggesting an exclusion property that acts among the nucleons sharing the same intrinsic state when embedded in an α cluster.

III. QUARTET QUANTUM PHASE TRANSITION IN INFINITE MATTER

So far, we have considered a QPT in ${}^{16}\text{O}$ as a function of the density where the nucleus changes from a homogeneous mean-field density spontaneously into a tetrahedral configuration of four α particles. However, those crystalline structures, imposed by the mean-field, become too high in energy. It is, for example, known that it is difficult to describe in detail the famous Hoyle state in ${}^{12}\text{C}$ at 7.65 MeV in this way. However effects of the Pauli principle and the density are already well described in mean-field theory as we demonstrate now. For dominant physical features in nuclei it is always very useful to consider the complimentary situation in infinite matter as has long been done, e.g., for nuclear pairing. Thus, we here want

to study quartet condensation and the corresponding QPT in infinite matter and make a link with the preceding mean-field study of ${}^{16}\text{O}$ concerning the typical densities at which the QPT occurs in nuclear systems. Quartet condensation is described following very closely the usual procedure of pairing with the BCS approach. For the latter the BCS equations can be written in the following way:

$$\begin{aligned}(e_{p_1} + e_{p_2})\kappa_{p_1 p_2} + (1 - n_{p_1} - n_{p_2}) \sum_{p'_1 p'_2} v_{p_1 p_2 p'_1 p'_2} \kappa_{p'_1 p'_2} \\ = 2\mu \kappa_{p_1 p_2},\end{aligned}\tag{3}$$

with the occupation numbers given by

$$n_k = \frac{1}{2} \left[1 - \frac{e_k - \mu}{\sqrt{(e_k - \mu)^2 + \delta_k^2}} \right],\tag{4}$$

with the gap

$$\Delta_k = g\kappa_{k\bar{k}},$$

where \bar{k} is the time-reversed state of k and we used as pairing force a δ interaction, $g\delta(\mathbf{r}_1 - \mathbf{r}_2)$. Finite-range forces can be treated accordingly.

In the above equations e_k are the kinetic energies, eventually with inclusion of a Hartree-Fock shift, and μ_i is the chemical potential. The indices p include momenta and spin, $\kappa_{p_1 p_2} = \langle c_{p_1} c_{p_2} \rangle$ is the pairing tensor, and $v_{p_1 p_2 p_3 p_4}$ is the matrix element of the pairing force. Equations (3) and (4) are the BCS equations in their general form. Usually one considers the Cooper pairs at rest, which makes the momenta of the two particles be opposite, and one considers spin singlet pairing.

For quartetting, one proceeds in a completely analogous way: one writes the in-medium four-body equation [64]

$$\begin{aligned}(e_1 + e_2 + e_3 + e_4)\kappa_{1234} + \sum_{1'2'3'4'} V_{1234;1'2'3'4'} \kappa_{1'2'3'4'} \\ = 4\mu \kappa_{1234},\end{aligned}\tag{5}$$

with

$$\begin{aligned}V_{1234;1'2'3'4'} = (1 - n_1 - n_2)v_{121'2'}\delta_{33'}\delta_{44'} \\ + (1 - n_1 - n_3)v_{131'3'} + \text{permutations},\end{aligned}\tag{6}$$

where we used an obvious shorthand notation. In the case of quartetting the expressions for the occupation numbers n_k are quite a bit more complicated with respect to the pairing case and we refer the reader to the literature [64]. To ease the numerical solution of the quartet equation, in Ref. [64], the four-nucleon order parameter was approximated by a mean-field ansatz projected to good total center of mass momentum $K = 0$ in the following way:

$$\langle c_{\mathbf{k}_1}^+ c_{\mathbf{k}_2}^+ c_{\mathbf{k}_3}^+ c_{\mathbf{k}_4}^+ \rangle = \delta(\mathbf{k}_1 + \mathbf{k}_2 + \mathbf{k}_3 + \mathbf{k}_4) \varphi(\mathbf{k}_1) \varphi(\mathbf{k}_2) \varphi(\mathbf{k}_3) \varphi(\mathbf{k}_4),\tag{7}$$

where $c_{\mathbf{k}}^+$ creates a nucleon with momentum \mathbf{k} (obvious spin-isospin indices are suppressed as well as the total scalar spin-isospin part of the wave function) and $\varphi(\mathbf{k})$ is a 0S single-particle wave function in momentum space. The self-consistent equation for the order parameter then boils down

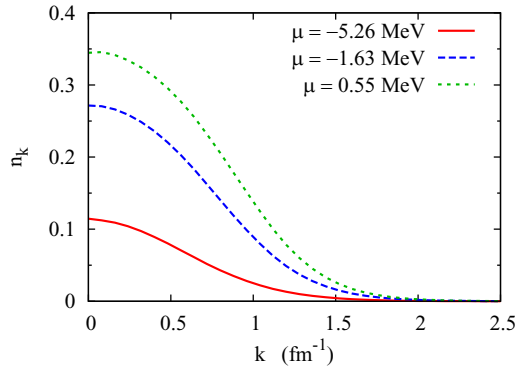


FIG. 10. Single-nucleon occupation numbers n_k for different values of μ . The highest value before the calculation of the α -order parameter breaks down is $\mu \approx 0.55$ MeV.

to a nonlinear equation for $\varphi(\mathbf{k})$ and it turns out that this approximation reproduces very well a full solution of the in-medium four-body equation [65]. The point now is that this order parameter only exists below a critical density of $\approx \rho_0/5$ [66], which is a value similar to the one found in the preceding study for ^{16}O . In infinite matter, this can then be qualified as a macroscopic QPT for quartets (α particles) with the density as a control parameter.

This breakdown was studied with the calculation of the single-nucleon occupation number n_k in the α condensate as a function of the chemical potential μ . We see in Fig. 10 that as μ increases, n_k naturally also increases. However, beyond $\mu \approx 0.55$ MeV where $n_{k=0} \approx 0.35$, the solution ceases to exist; that is, the α order parameter has disappeared and the system has turned over into a standard nuclear superfluid very analogous to what we have seen happening in ^{16}O . It should be pointed out that this behavior is in strong contrast to pairing, for instance, deuteron pairing, where the density can be increased without breakdown of superfluidity, the decrease of the gap being only commended by the finite range of the pairing force. The corresponding n_k values steadily increase from negative to positive values of μ without interruption. Of course the Pauli principle forbids that n_k overshoots the value of 1 (disregarding spin and isospin degeneracies), reaching the typical BCS-like behavior at nuclear saturation densities. This behavior is shown in Fig. 11 in a qualitative way. We see the strong difference with the behavior of n_k in the quartet case. It should be noted that the distributions below and around $\mu \simeq 0$ should be compared with the ones of the quartet case.

The reason for this breakdown has a simple physical interpretation. It seems clear that in a four-body problem the in-medium four-body level density plays a dominant role. It is defined by [67]

$$g_4(\omega) = \sum_{k_1, k_2, k_3, k_4} [\bar{f}_1 \bar{f}_2 \bar{f}_3 \bar{f}_4 - f_1 f_2 f_3 f_4] \times \delta(\omega - e_1 - e_2 - e_3 - e_4), \quad (8)$$

where $\bar{f} = 1 - f$ and $f_i = f(e_i)$ is the Fermi-Dirac function equal to $\Theta(\mu - e_i)$ at zero temperature. The e_i 's are the kinetic energies $p_i^2/(2m)$. One can easily verify that for positive chemical potential μ , this four-body level density goes

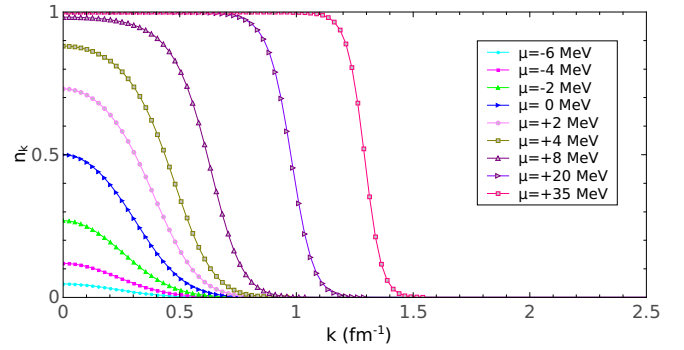


FIG. 11. Schematic (non-self-consistent) view of BCS occupation numbers as the chemical potential varies from positive to negative (binding) values.

through zero at $\omega = 4\mu$. Where there is no level density at the Fermi surface no correlations can develop and, thus, the order parameter goes to zero very soon after μ has turned from negative values (binding) to positive ones (scattering).

The critical density coincides with the Mott density at zero temperature [66]. Actually the critical density is just the one where the α 's start to overlap with their tails to some appreciable extent (see, e.g., the two α 's in ^8Be [68]) and, thus, the Pauli principle becomes active. For the pairing case, for two particles at rest with their c.m., one verifies that the two-body level density is finite at $\omega = 2\mu$, this being the reason why pairing also exists for positive μ or at high densities. For example, the two-body level density for two particles below 2 times the chemical potential is given by

$$g(\omega)_{2p} = \sum_{k_1 k_2} \Theta(\mu - e_{k_1}) \Theta(\mu - e_{k_2}) \delta(\omega - e_{k_1} - e_{k_2}). \quad (9)$$

For the particle pair at rest, $k_1 = k_2$, one easily verifies that for $\omega = 2\mu$ the level density is finite. On the contrary, if the two nucleons are moving with a finite center-of-mass momentum, also a hole develops at the Fermi level similar to what we have seen for the three-particle case. The width of this hole increases with increasing center-of-mass momentum until the gap disappears. This signals the critical center-of-mass momentum. The finiteness of the level density at the Fermi level for two particles at rest is unique for the case of many-body level densities. This is the reason why pairing is such a unique phenomenon.

In conclusion, we have seen in this section that the density dependence of α condensation in infinite matter is somewhat lower but still in line with the mean-field studies in the finite nuclei presented above. This means in particular that the action of the Pauli principle on the existence of α clusters is similar in infinite matter and finite nuclei. As mentioned above the density of the Hoyle state is $\rho_0/3 - \rho_0/4$, very close to the mean-field values in this study. In Ref. [69], for the hypothetical four- α condensate state in ^{16}O at 15.1 MeV the calculation yields quite a bit a lower density close to $\rho_0/6$. However, the four- α calculation is more involved and the density of the condensate may not be calculated with the the same precision as in the case of three α 's; that is, the value $\rho_0/6$ may

be somewhat uncertain. Also the four- α calculation may be more sensitive to small perturbations like the increased (with respect to the ^{12}C case) Coulomb repulsion.

IV. CONCLUSIONS

In conclusion, we have studied in nuclear systems the transition from a Fermi gas to α clustering as a function of density at zero temperature. In a first study we made constrained HFB calculations, both with RMF and Gogny EDFs, where the radius of ^{16}O is increased under the constraint that on average the system stays spherical, that is, that the mean value of the quadrupole operator remains zero. The system shows a critical radius, i.e., low density where the homogeneously inflated ^{16}O nucleus abruptly goes over into a tetrahedral configuration of four α 's. This happens consistently with the relativistic and nonrelativistic approaches at practically the same critical density $\approx \rho_0/3$, slightly higher than in the infinite matter calculation where the phase transition from the Fermi gas to α -particle condensation happens at $\rho_{\text{Mott}} = 0.03 \text{ fm}^{-3} \approx$

$\rho_0/5$ [64,66]. This shows that the Pauli principle that triggers this QPT transition acts rather similarly, independently of whether the system goes over into a condensate or a lattice configuration as this happens with the constrained mean-field calculation for ^{16}O . We further investigated the transition to four α 's in ^{16}O . We expressed the nondynamical correlations grasped through the SSB of the O(3) rotation group down to the point group T_d in terms of p-h excitations on top of a symmetry-preserving SD, and we discussed the crucial role played by orbitals beyond the p and sd shells to localize nucleons into α 's at the corners of a tetrahedron. All in all, ^{16}O provides a rather spectacular example of a quantum phase transition in nuclear physics.

ACKNOWLEDGMENTS

P.S. thanks G. Roepke for useful discussions. This publication is based on work supported in part by the framework of the Espace de Structure et de réactions Nucléaires Théorique (ESNT) at CEA.

-
- [1] J. R. Williams, E. L. Hazlett, J. H. Huckans, R. W. Stites, Y. Zhang, and K. M. O'Hara, *Phys. Rev. Lett.* **103**, 130404 (2009).
 - [2] Y. Nishida, *Phys. Rev. Lett.* **109**, 240401 (2012).
 - [3] C. Wu, J.-P. Hu, and S.-C. Zhang, *Phys. Rev. Lett.* **91**, 186402 (2003).
 - [4] S. Capponi, G. Roux, P. Lecheminant, P. Azaria, E. Boulat, and S. R. White, *Phys. Rev. A* **77**, 013624 (2008).
 - [5] T. Bourdel, L. Khaykovich, J. Cubizolles, J. Zhang, F. Chevy, M. Teichmann, L. Tarruell, S. J. J. M. F. Kokkelmans, and C. Salomon, *Phys. Rev. Lett.* **93**, 050401 (2004).
 - [6] A. Gezerlis, G. F. Bertsch, and Y. L. Luo, *Phys. Rev. Lett.* **106**, 252502 (2011).
 - [7] S. Frauendorf and A. O. Macchiavelli, *Prog. Part. Nucl. Phys.* **78**, 24 (2014).
 - [8] G. Röpke, L. Münchow, and H. Schulz, *Nucl. Phys. A* **379**, 536 (1982).
 - [9] G. Röpke, A. Schnell, P. Schuck, and P. Nozières, *Phys. Rev. Lett.* **80**, 3177 (1998).
 - [10] C. J. Horowitz and A. Schwenk, *Nucl. Phys. A* **776**, 55 (2006).
 - [11] A. Tohsaki, H. Horiuchi, P. Schuck, and G. Röpke, *Phys. Rev. Lett.* **87**, 192501 (2001).
 - [12] T. Yamada and P. Schuck, *Phys. Rev. C* **69**, 024309 (2004).
 - [13] T. Yamada, Funaki, H. Horiuchi, G. Röpke, P. Schuck, and A. Tohsaki, *Clusters Nucl.* **2**, 229 (2012).
 - [14] M. Girod and P. Schuck, *Phys. Rev. Lett.* **111**, 132503 (2013).
 - [15] J.-P. Ebran, E. Khan, T. Nikšić, and D. Vretenar, *Phys. Rev. C* **89**, 031303(R) (2014).
 - [16] S. Elhatisari *et al.*, *Phys. Rev. Lett.* **117**, 132501 (2016).
 - [17] M. Freer, *Rep. Prog. Phys.* **70**, 2149 (2007).
 - [18] M. Freer, H. Horiuchi, Y. Kanada-Enyo, D. Lee, and Ulf-G. Meißner, *Rev. Mod. Phys.* **90**, 035004 (2018).
 - [19] P. Marević, J.-P. Ebran, E. Khan, T. Nikšić, and D. Vretenar, *Phys. Rev. C* **97**, 024334 (2018).
 - [20] P. Marević, J.-P. Ebran, E. Khan, T. Nikšić, and D. Vretenar, *Phys. Rev. C* **99**, 034317 (2019).
 - [21] P. Schuck, *J. Phys.: Conf. Ser.* **436**, 012065 (2013), and references therein.
 - [22] J.-P. Ebran, E. Khan, T. Nikšić, and D. Vretenar, *Phys. Rev. C* **90**, 054329 (2014).
 - [23] C. L. Zhang, B. Schuetrumpf, and W. Nazarewicz, *Phys. Rev. C* **94**, 064323 (2016).
 - [24] R. Bijker and F. Iachello, *Phys. Rev. Lett.* **112**, 152501 (2014).
 - [25] J. Bishop, T. Kokalova, M. Freer, L. Acosta, M. Assie, S. Bailey *et al.*, *Phys. Rev. C* **100**, 034320 (2019).
 - [26] S. Ohkubo, J. Takahashi, and Y. Yamanaka, *Prog. Theor. Exp. Phys.* **2020**, 041D01 (2020).
 - [27] Y. Funaki, A. Tohsaki, H. Horiuchi, P. Schuck, and G. Röpke, *Phys. Rev. C* **67**, 051306(R) (2003).
 - [28] M. Chernykh, H. Feldmeier, T. Neff, P. von Neumann-Cosel, and A. Richter, *Phys. Rev. Lett.* **98**, 032501 (2007).
 - [29] J. Eichler and A. Faessler, *Nucl. Phys. A* **157**, 166 (1970).
 - [30] M. Girod and B. Grammaticos, *Phys. Rev. C* **27**, 2317 (1983).
 - [31] P. Arumugam, B. K. Sharma, S. K. Patra, and R. K. Gupta, *Phys. Rev. C* **71**, 064308 (2005).
 - [32] J. A. Maruhn, M. Kimura, S. Schramm, P. G. Reinhard, H. Horiuchi, and A. Tohsaki, *Phys. Rev. C* **74**, 044311 (2006).
 - [33] A. S. Umar, J. A. Maruhn, N. Itagaki, and V. E. Oberacker, *Phys. Rev. Lett.* **104**, 212503 (2010).
 - [34] T. Ichikawa, J. A. Maruhn, N. Itagaki, and S. Ohkubo, *Phys. Rev. Lett.* **107**, 112501 (2011).
 - [35] T. Ichikawa, Y. Kanada-Enyo, and P. Moller, *Phys. Rev. C* **83**, 054319 (2011).
 - [36] P.-G. Reinhard, J. A. Maruhn, A. S. Umar, and V. E. Oberacker, *Phys. Rev. C* **83**, 034312 (2011).
 - [37] L. M. Robledo and G. F. Bertsch, *Phys. Rev. C* **84**, 054302 (2011).
 - [38] J.-P. Ebran, E. Khan, T. Nikšić, and D. Vretenar, *Nature (London)* **487**, 341 (2012).
 - [39] J.-P. Ebran, E. Khan, T. Nikšić, and D. Vretenar, *Phys. Rev. C* **87**, 044307 (2013).
 - [40] S. Typel, *Phys. Rev. C* **89**, 064321 (2014).
 - [41] B. Schuetrumpf and W. Nazarewicz, *Phys. Rev. C* **96**, 064608 (2017).

- [42] J.-P. Ebran, E. Khan, R.-D. Lasserri, and D. Vretenar, *Phys. Rev. C* **97**, 061301(R) (2018).
- [43] Z. X. Ren, P. W. Zhao, and J. Meng, *Phys. Lett. B* **801**, 135194 (2020).
- [44] G. A. Lalazissis, T. Nikšić, D. Vretenar, and P. Ring, *Phys. Rev. C* **71**, 024312 (2005).
- [45] G. M. King, *J. Phys. A: Math. Nucl. Gen.* **6**, 901 (1973).
- [46] G. Rosensteel and J. P. Draayer, *J. Phys. A: Math. Gen.* **22**, 1323 (1989).
- [47] D. Bhaumik *et al.*, *J. Phys. A: Math. Gen.* **27**, 1401 (1994).
- [48] W. Nazarewicz and J. Dobaczewski, *Phys. Rev. Lett.* **68**, 154 (1992).
- [49] M. Freer, R. R. Betts, and A. H. Wuosmaa, *Nucl. Phys. A* **587**, 36 (1995).
- [50] J. F. Berger, M. Girod, and D. Gogny, *Comput. Phys. Commun.* **63**, 365 (1991).
- [51] N. Onishi and R. K. Sheline, *Nucl. Phys. A* **165**, 180 (1971).
- [52] G. Ripka, *J. Phys. Colloq.* **32**, C6-261 (1971).
- [53] K. Ananthanarayanan, S. Das Gupta, and N. De Takacsy, *Phys. Lett. B* **37**, 143 (1971).
- [54] C. Abulaffio and J. M. Irvine, *Phys. Lett. B* **38**, 492 (1972).
- [55] D. Robson, *Phys. Rev. Lett.* **42**, 876 (1979).
- [56] D. Robson, *Phys. Rev. C* **25**, 1108 (1982).
- [57] W. Bauhoff, H. Schultheis, and R. Schultheis, *Phys. Rev. C* **29**, 1046 (1984).
- [58] C. J. Halcrow, C. King, and N. S. Manton, *Int. J. Mod. Phys. E* **28**, 1950026 (2019).
- [59] P. W. Atkins, M. S. Child, and C. S. G. Phillips, *Tables for Group Theory* (Oxford University, Oxford, 1970).
- [60] J. Dudek, A. Gozdz, N. Schunck, and M. Miskiewicz, *Phys. Rev. Lett.* **88**, 252502 (2002).
- [61] J. Dudek, A. Gozdz, H. Moliq, and D. Curien, *J. Phys.: Conf. Ser.* **413**, 012001 (2013).
- [62] J. Dudek, D. Curien, I. Dedes, K. Mazurek, S. Tagami, Y. R. Shimizu, and T. Bhattacharjee, *Phys. Rev. C* **97**, 021302(R) (2018).
- [63] R. S. Mulliken, *Science* **157**, 13 (1967).
- [64] T. Sogo, G. Röpke, and P. Schuck, *Phys. Rev. C* **81**, 064310 (2010).
- [65] T. Sogo, R. Lazauskas, G. Röpke, and P. Schuck, *Phys. Rev. C* **79**, 051301(R) (2009).
- [66] G. Röpke, P. Schuck, Y. Funaki, H. Horiuchi, Z. Ren, A. Tohsaki, C. Xu, T. Yamada, and B. Zhou, *Phys. Rev. C* **90**, 034304 (2014).
- [67] A. H. Blin, R. W. Hasse, B. Hiller, P. Schuck, and C. Yannouleas, *Nucl. Phys. A* **456**, 109 (1986).
- [68] R. B. Wiringa, S. C. Pieper, J. Carlson, and V. R. Pandharipande, *Phys. Rev. C* **62**, 014001(R) (2000).
- [69] B. Zhou, Y. Funaki, H. Horiuchi, and A. Tohsaki, *Front. Phys.* **15**, 14401 (2019).